HHS Public Access

Author manuscript

Exp Neurol. Author manuscript; available in PMC 2022 February 01.

Published in final edited form as:

Exp Neurol. 2021 February ; 336: 113537. doi:10.1016/j.expneurol.2020.113537.

Intrauterine growth restriction compromises cerebellar development by affecting radial migration of granule cells via the *JamC/Pard3a* molecular pathway

Igor Y. Iskusnykh[1,*], **Nikolai Fattakhov**[1], **Randal K. Buddington**[2,3,4], **Victor V. Chizhikov**[1,*]

[1]Department of Anatomy and Neurobiology, University of Tennessee Health Science Center, Memphis, TN 38163, USA

[2]Babies Taking Flight, Memphis, TN 38117, USA

[3]School of Health Studies, University of Memphis, Memphis, TN 38152, USA

[4]College of Nursing, University of Tennessee Health Science Center, Memphis, TN 38163, USA

Abstract

Intrauterine growth restriction (IUGR) affects ~10% of human pregnancies, results in infants born small for gestational age (SGA), and is associated with motor and cognitive deficits. Human studies suggest that some deficits in SGA patients originate in the cerebellum, a major motor-coordination and cognitive center, but the underlying mechanisms remain unknown. To identify the cerebellar developmental program affected by IUGR, we analyzed the pig as a translational animal model in which some fetuses spontaneously develop IUGR due to early-onset chronic placental insufficiency. Similar to humans, SGA pigs revealed small cerebella, which contained fewer mature granule cells (GCs) in the internal granule cell layer (IGL). Surprisingly, newborn SGA pigs had increased proliferation of GC precursors in the external granule layer (EGL), which was associated with an increased density of Purkinje cells, known to non-autonomously promote the proliferation of GCs. However, the GCs of SGA pigs did not properly initiate exit from the EGL to IGL, which was associated with a decreased density of guiding Bergmann glial fibers, reduced expression of pro-migratory genes *Pard3a, JamC* and *Sema6a*, and increased apoptosis. While proliferation spontaneously normalized during postnatal development, accumulation of pre-migratory GCs and apoptosis in the EGL were long-lasting consequences of IUGR. Using organotypic cerebellar slice cultures, we showed that normalizing expression of *Pard3a* and *JamC*, which operate in the same molecular pathway in GCs, was sufficient to rescue both migratory and, at a later time point, apoptotic defects of IUGR. Thus, a decreased exit of GCs from the EGL, due

*Corresponding authors at: University of Tennessee Health Science Center, Department of Anatomy and Neurobiology, 855 Monroe Ave, Link Building, Ste 515, Memphis, TN 38163, iiskusny@uthsc.edu, vchizhik@uthsc.edu.

Author Contributions:

I.Y.I., R.K.B, and V.V.C. designed the study; I.Y.I and N.F. performed experiments and analyzed data; R.K.B. and V.V.C. supervised the study; I.Y.I and V.V.C. wrote the paper.

Conflict of Interests:

The authors declare no competing interests.

to disrupted Pard3a/JamC radial migration initiation pathway, is a major mechanism of IUGR-related cerebellar pathology.

Keywords

intrauterine growth restriction; cerebellum; development; translational large animal model; pig; neuronal migration; neurogenesis; proliferation; apoptosis; developmental brain disorder; cerebellar hypoplasia

Introduction

Intrauterine growth restriction (IUGR), a condition of reduced fetal growth, results in infants born small for gestation age (SGA). Typically, IUGR is diagnosed when body weight is below the 10th percentile for gestational age (Devaskar and Chu, 2016). In humans, IUGR has multiple causes, including genetic or environmental factors, but most commonly arises because of placental insufficiency that frequently develops early in pregnancy (Rozance et al., 2016). Placental insufficiency leads to fetal undernutrition and hypoxia, affecting embryonic development by altering tissue-specific gene expression programs (Brown and Hay, 2016).

IUGR is the second leading cause of infant mortality and morbidity (after preterm birth) and is associated with impaired motor and cognitive functioning (Miller et al., 2016; Vollmer and Edmonds, 2019). Since the cerebellum is the primary center of motor-coordination and contributes to cognition (Koziol et al., 2014), it has been hypothesized that some neurological deficits in subjects born SGA result from disrupted cerebellar development (Miller et al., 2016; Wang et al., 2016).

Cerebellar development begins in the first trimester of pregnancy, when two germinal zones are formed: the rhombic lip, which gives rise to granule cells (GCs), and the ventricular zone, which generates Purkinje cells (Butts et al., 2014; Basson and Wingate, 2013; Haldipur et al., 2018). GCs exit the rhombic lip, forming the external granule cell layer (EGL), where they proliferate in response to Shh-signaling from Purkinje cells (Chizhikov and Millen, 2020). Upon differentiation, GCs migrate radially along Bergmann glial fibers to form the internal granule cell layer (IGL). Radial migration of GCs is critical for the establishment of proper cerebellar cytoarchitecture and circuitry formation (Sillitoe and Joyner, 2007).

The prolonged prenatal development makes the human cerebellum vulnerable to an adverse intrauterine environment. Indeed, a decreased cerebellar size was reported in patients born SGA. (Caetano et al., 2015; De Bie et al., 2011). However, the developmental mechanisms affected by IUGR remain largely unknown, preventing development of therapeutic strategies for patients affected by IUGR.

Recently, several studies analyzed cerebellar histology in animals with IUGR induced by uterine artery ligation in late pregnancy (McDougal et al., 2017; Yawno et al., 2019). Notably, abrupt disruption of fetal-maternal communication caused by uterine artery ligation

is different from the placental insufficiency that gradually develops in many human patients, frequently from early pregnancy stages (Bamfo and Odibo, 2011; Herrera et al., 2016). Also, the cerebellar growth spurt in humans begins *in utero*, whereas in rodents, which dominate IUGR studies (McDougall et al., 2017; Tolcos et al., 2018), the cerebellum grows predominantly after birth (Haldipur et al., 2018; 2019). Thus, analysis of a translational animal model is necessary to identify the effects of early-onset, chronically-developing placental insufficiency on cerebellar development.

In all modern breeds of the domestic pig, because of heterochronic implantation and competition for uterine space, some fetuses spontaneously develop IUGR. SGA pig fetuses, which can be identified from the first trimester of pregnancy, have small placentae with a reduced transporting capacity (Ashworth et al., 2001; Wang et al., 2017; Matheson et al., 2018). Importantly, pigs share a cerebellar developmental trajectory with humans (Iskusnykh et al., 2018). Thus, the pig is an excellent, well-established model to study IUGR caused by chronically-developing early-onset placental insufficiency (Ashworth et al., 2001; Radlowski et al., 2014).

Using the pig as a translational animal model, we demonstrate that early-onset IUGR affects GCs, Purkinje cells, and Bergmann glia. While GC overproliferation, associated with an increased density of Purkinje cells, was a transient abnormality in SGA pigs, accumulation of pre-migratory GCs and their apoptosis in the EGL were long-lasting consequences of IUGR. Our gene expression and slice electroporation experiments revealed that IUGR reduces expression of *Pard3a* and *JamC*, which belong to the same pro-migratory pathway, and that restoring expression of these genes was sufficient to rescue IUGR-induced GC migratory and apoptotic defects. We, thereby, identify the first major molecular mechanism that underlies cerebellar pathology in this common human condition.

Materials and Methods

Experimental design, pigs, and brain collection.

All experiments with live animals were conducted following the protocols approved by the University of Memphis or the University of Tennessee Health Science Center Institutional Animal Care and Use Committees. Newborn pigs were obtained from artificially inseminated sows of a consistent genetic lineage maintained at a commercial facility. Consistently with previous studies (Miller et al., 2016; Sharma et al., 2016) we considered newborn pigs with body mass less than 0.9 kg (average weight 0.75±0.09 kg, range from 0.6 to 0.88 kg), which correspond to the lowest body weight 10th percentile, small for gestational age (SGA). The SGA pigs originated from multiple litters, and littermates of normal birthweight (normal for gestational age, NGA), (body weight 1.64±0.22 kg, range 1.24 to 1.99 kg) were used as controls. Pigs were euthanized either within 12 hours after birth (at postnatal day 0, P0 pigs) or after rearing for 20 days (P20 pigs) in AAALAC accredited facilities using a commercially available milk replacement (Buddington et al., 2018). Both males and females were used in the study. All animals had normal physical appearance and behavior at the time of necropsy. On macroscopic and microscopic examination, none of the brains had evidence of injury.

Immediately after euthanasia, the entire brain was removed, and the cerebellum was cut sagittally into ~0.5 cm thick slices that were processed for immunohistochemistry, *ex-vivo* slice culture experiments or laser capture microdissection.

Immunohistochemistry.

Upon collection, cerebella were fixed in 4% paraformaldehyde (PFA) at 4° C for 48 h, washed in PBS three times, sunk in 30% sucrose in PBS, and embedded in OCT (optimum cutting temperature) compound. The OCT blocks were sectioned sagittally on a Leica CM3050 cryostat. Sections were mounted on Superfrost Plus slides. Immunohistochemistry with all antibodies, except anti-BrdU and anti-Ki67 antibodies, was performed following our previous protocols (Iskusnykh et al., 2016; Chizhikov et al., 2019). Slides were dried for 20 min at room temperature, washed in PBS (3 times, 10 min each), and blocked with 1% heat-inactivated goat serum and 0.1% Triton X100 in PBS for 1 h at room temperature. Then, slides were incubated for 10 h at 4° C with primary antibodies followed by species-appropriate Alexa Fluor 594 conjugated secondary antibodies (Invitrogen, USA) for 1 h at room temperature. Anti-Ki67 and anti-BrdU immunostaining was performed as described above, except after washing in PBS, slides were boiled in 1X antigen retrieval solution (Sigma) for 10 min. Primary antibodies included rabbit anti-Calbindin D-28k (Swant, catalog #CB-38, dilution1:200), mouse anti-NeuN clone A60 (Sigma Aldrich, catalog # MAB377, dilution 1:500), rabbit anti-Pax6 (BioLegend, catalog # Prb-278p-100, dilution 1:350), rabbit anti-GFAP (Dako, catalog # Z0334, dilution 1:200), mouse anti-Ki67 clone B56 (BD Pharmingem, catalog # 556003, dilution 1:250), rat anti-phospho histone H3 (Abcam, catalog # ab90543, dilution 1:200), rabbit anti-cleaved Caspase-3 (Cell Signaling, catalog # 9664, dilution 1:300), mouse anti-Tag1 (Developmental Studies Hybridoma Bank, University of Iowa, dilution1:5), and rabbit anti-BrdU (Rockland, catalog # 600–401-C29S, dilution 1:300). DAPI staining was used to identify cell nuclei and to assess gross tissue morphology.

Ex-vivo organotypic cerebellar slice culture experiments.

Organotypic slices obtained from SGA and NGA pig cerebella were used to study GC migration. Cerebellar slices were prepared from P0 pigs as previously described (Iskusnykh et al., 2018). Briefly, blocks of cerebellar vermes were embedded in 4% low temperature melting agarose in Krebs buffer (pH=7.2) and sagittally sliced on a vibratome at 400 μm. Slices were transferred to Millicell cell culture inserts (0.4 μm pore size, Millipore, USA), which were placed on the surface of DMEM medium (Invitrogen, USA) containing glutamine, glucose, 10% fetal calf serum, and Penicillin/Streptomycin, and then incubated in a CO_2 incubator at 37°C with 5% CO_2 for 1 h (Daza et al., 2007; Englund et al., 2006). Then, the DMEM medium was changed to a serum-free neurobasal/B27 medium (Invitrogen, USA) with BrdU (1:1000 dilution of the BrdU labeling reagent, Thermo Fisher Scientific, cat # 000103). After a 6 h exposure to label dividing GC precursors in the EGL, the BrdU-containing medium was replaced with BrdU-free medium of the same composition. Then, 24 h or 48 h after the beginning of the incubation, slices were rinsed in PBS three times (30 min each), fixed in 4% PFA in PBS at 4° C for 1.5 h, cryoprotected using 30% sucrose solution in 1x PBS at 4° C, and embedded in OCT compound. OCT

blocks were sectioned on a Leica CM3050 cryostat and used for immunohistochemistry, which was performed as described above for cerebellar tissue analysis.

Ex vivo cerebellar electroporation.

P0 cerebella were removed from the skull, separated from the meninges, cut into 0.5 cm thick pieces, and placed into a Petri dish platinum electrode chamber (Btx, cat # 45–0505) filled with endotoxin-free plasmid DNA in complete Hanks Balanced Salt Solution (Gibco, USA). The EGL was oriented toward the negative electrode to facilitate the negatively-charged plasmid DNA moving toward the positive electrode to enter GC precursors superficially located in the EGL (Famulski et al., 2010; Renaud and Chédotal, 2014). To visualize transfected cells, in all experiments a vector encoding nuclear mCherry (*pCIG2-H2B-mCherry*) was electroporated alone or co-electroporated with *pCIG2-JamC* and/or *pCIG2-Pard3a* expression plasmids (Famulski et al., 2010). Electroporations were performed using 5 pulses (120 V, 50 ms each, 500 ms interval between pulses) delivered via an ECM630 electroporator (Btx, Harvard Apparatus). After the electroporation, cerebella were embedded in 4% low temperature melting agarose, sagittally sliced on a vibratome at 400 μm and cultured *ex vivo* for 36 h or 48 h as described above for organotypic cerebellar slices (except no BrdU was added to the medium). After fixing slices in 4% PFA, embedding in OCT, and sectioning at a cryostat, electroporated cells were identified based on mCherry fluorescence.

Laser Capture Microdissection (LCM) and qRT-PCR.

Fresh cerebellar tissue blocks were embedded in OCT on dry ice. Tissue was sectioned using a Leica cryostat, and 10 μm thick sections were collected on plain glass slides. For the EGL visualization, fresh frozen tissue sections were dehydrated using ethanol and stained with Cresyl violet in 50% EtOH for 30 sec. The sections were dehydrated again in ethanol and xylene. After drying for 5 min at room temperature, entire EGL (blue layer in Fig. 3D and diagram in Fig. 5) was isolated by LCM from five sections of each cerebellar vermis, using an Arcturus XT machine with CapSure Macro Caps (Arcturus, USA). RNA was extracted with a PicoPure™ RNA Isolation Kit (Arcturus, San Diego, CA), according to the manufacturer's instructions. RNase-Free DNase Set (Cat #79256, Qiagen) was used to remove traces of the genomic DNA absorbed on columns, prior to RNA elution. RNA samples with the RNA integrity number (RIN) higher than eight were used for qRT-PCR analysis. Reverse transcription of RNA was performed with the iSciptTM cDNA Synthesis Kit (Biorad, USA). Amplification was performed using the Roche LightCycler 480 machine and KAPA SYBR FAST qPCR Master Mix Kit as described previously (Currle et al., 2005; Yoo et al., 2014). Relative gene expression was calculated by the 2-ΔΔCT method (Livak et al., 2001). The expression of each gene was normalized against *Gapdh*. The primers used are listed below:

JamC F: TACAGCTGGTACCGCAATGA and *JamC* R: GAATCTGGGGTTGGCTCTG

Pard3a F: GCTTCCAGAGTGCCAAAGAG and *Pard3a* R: AGCCATGTCCTCCCAGGTA

Sema 6A F: GTAACTGCCTGCAGTATGTTGAA and

Sema 6A R: CTTAAGGCTCGCCTCAACTG

Astn1 F: GGGAGTGGACAACACAGGTC and *Astn1* R: CTTTGACATCGTCCACCACA

Cxcr4 F: CGCAAAGCTCTCAAAACCAC and *Cxcr4* R: GAGGATGAAGGAGTCGATGC

Barhl 1 F: GGCCTTCACAGACCATCAG and *Barhl 1* R: TGCACGCTCAGGTACTTCTG

Plexin A2 F: GCTCACGCTCACCAACAA and *Plexin A2* R: CAGCCGGTTCTCGGAGTAG

Ptch1 F: GCGTGGATGATGTTTTCCTT and *Ptch1* R: GCTTGAGGCATTCTCCAGTC

Gli1 F: CAGGGAGGAGAGCAGACTGA and *Gli1* R: TCACTGCTGCAGGAGGACT

Gapdh F: ACCCAGAAGACTGTGGATGG and *Gapdh* R: AAGCAGGGATGATGTTCTGG

qPCR reactions were performed in triplicate. Data are presented as the means ± sd. Comparisons between SGA and NGA pigs were made using the two-tailed Student's t-test, with $p<0.05$ considered statistically significant.

Cell counts, measurements, and statistical analysis.

The numbers of Pax6+, Ki67+, and NeuN+ GC precursors in the EGL, GFAP+ Bergmann glial fibers in the ML, and NeuN+ GCs in the IGL were determined using the optical fractionator method with 20 μm-thick sections. Z-stack images with 1 μm optical step were obtained using a Zeiss LSM 710 confocal microscope and uploaded into the Stereo Investigator Software for an unbiased cell count analysis as previously described (Iskusnykh et al., 2018; Glaser et al., 2007). The number of Ki67+, Pax6+, and NeuN+ cells was calculated in 100 μm-long segments of the EGL with 15 μm dissector height. The number of GFAP+ Bergmann glial fibers was evaluated in 200 μm x 200 μm squares of the molecular layer with 12 μm dissector height. The number of NeuN+ cells in the IGL was calculated in lobes III and VIII of the cerebellar vermis. First, the density of NeuN+ cells in the IGL was calculated in 100 μm x 100 μm squares with 12 μm dissector height. Then, GC counts per lobe were obtained by multiplying the density of NeuN+ cells in the IGL and IGL volume for a particular lobe in each section. For clarity, the numbers of NeuN+ cells in the IGL of each lobe in SGA pigs were normalized to those in NGA pigs, which were set as 1.

The thickness of Tag1+ layer, the number and diameter of (Calb+) Purkinje cells, the numbers of histone H3 (pH3+) and activated caspase 3 (act Casp+) - positive cells were estimated using 12 μm-thick sections, which were captured by Zeiss A2 fluorescent Microscope equipped with Zeiss AxioCam MRm camera. The measurements were performed using Image J software (NIH) as previously described (Iskusnykh et al., 2018). Purkinje cells were counted along the 500 μm line drawn parallel to the Purkinje cell layer. Purkinje cell diameter was measured in 40 randomly selected Purkinje cells in lobes III and VIII of the cerebellar vermis. The numbers of mitotic pH3+ cells were measured per 1 mm of the EGL; the numbers of apoptotic (act Casp+) cells were measured per 1 mm of the EGL or per $1mm^2$ of the ML and IGL (Zhang et al., 2015; Fauquier et al., 2014).

For migration experiments using cerebellar slices, the distance of mCherry+ or BrdU+ cells was measured from the outer surface of the EGL using ImageJ (NIH) software.

For consistency, all measurements and cell counts in NGA and SGA cerebella were performed in sections (or slices) taken from medial cerebellar vermis. At least three NGA and three SGA cerebella (three sections per cerebellum) at each developmental stage were analyzed for each marker. All data are presented as means ± sd. Statistical significance was determined by either a two-tailed t-test (when two experimental conditions were compared) or by one-way ANOVA with Tukey's post hoc test (when more than two experimental conditions were compared); $p<0.05$ was considered statistically significant for all comparisons.

Results

Intrauterine growth restriction reduces the numbers of differentiated granule cells and Bergmann glia, but increases the density of Purkinje cells at birth.

To determine whether IUGR caused by chronic placental insufficiency affects cerebellar development, we compared pigs naturally born SGA with normal for gestational age (NGA) littermates. SGA pigs had significantly ($p=7.4\times10^{-5}$) reduced average cerebellar weight compared to NGA littermates on the day of birth (P0) (Fig. 1A). To determine cerebellar populations affected by IUGR, we quantified mature GCs in the IGL and also Purkinje cells and Bergmann glial fibers at P0, using cell-type-specific markers NeuN (to identify differentiated GCs), Calbindin (to identify Purkinje cells), and GFAP (to identify Bergmann glia) (Iskusnykh et al., 2018; Swanson et al., 2010; Yeung et al., 2016).

The number of NeuN+ GCs in the IGL was reduced in both the anterior (lobe III, $p=0.045$) and posterior (lobe VIII, $p=0.049$) cerebellum of SGA pigs relative to NGA controls (Fig. 1B–J). In contrast, the density of Purkinje cells was increased in SGA pigs ($p=0.019$ and $p=0.018$ for the anterior and posterior cerebellum, respectively) (Fig. 1K–N), while the diameter of Purkinje cells was smaller in SGA pigs compared to NGA controls ($p=0.0032$) (Fig. 1K, L, O). The density of Bergmann glial fibers was reduced in both the anterior ($p=0.006$) and posterior ($p=0.026$) cerebellum of SGA pigs (Fig. 1P–S). Thus, spontaneous IUGR in the pig affects multiple cell types, resulting in a decreased number of GCs in the IGL, decreased density of Bergmann glial fibers, and reduced diameter of Purkinje cells, but increases the density of Purkinje cells in P0 cerebellum.

Excessive accumulation of undifferentiated and differentiating granule cell precursors in the EGL of newborn SGA pigs.

GCs, which are the most numerous neurons in the entire brain, are critical for the proper functioning of the cerebellum and constitute a large fraction of the cerebellar weight and volume (Sillitoe and Joyner, 2007; Leto et al., 2016; Chizhikov and Millen, 2020). The decreased cerebellar weight and reduced number of differentiated GCs in the IGL led us to investigate the mechanisms underlying the compromised GC development associated with IUGR, beginning with the analysis of GC precursors in the EGL.

GC precursors proliferate in the EGL, where undifferentiated cells occupy the outer EGL, while differentiating GC precursors move to the inner EGL, before migrating to the IGL (Faust, 2003; Chizhikov et al., 2007). Immunohistochemistry for Pax6, which is expressed in both undifferentiated and differentiating GC precursors, revealed an increased number of GC precursors in the EGL of P0 SGA pigs in both anterior (lobe III, p=0.0008) and posterior (lobe VII, p=0.034) cerebellum (Fig. 2A–D). The number of undifferentiated (Ki67+) GC precursors was only modestly increased in both anterior and posterior SGA cerebellum (by ~12% and ~18%, p=0.044 and p=0.034, respectively) (Fig. 2E–H). Interestingly, there was a much more pronounced increase in the number of differentiating pre-migratory (NeuN+) GCs in the EGL of P0 SGA pigs relative to NGA controls (by ~64%, in anterior cerebellum and by 41%, in posterior cerebellum, p=0.0011 and p=0.04, respectively) (Fig. 2I–L). Also, Tag1+ inner EGL, which contains pre-migratory differentiating GCs (Chizhikov et al., 2007), was much thicker in SGA relative to NGA cerebella (increased by ~51% in anterior cerebellum and by 64% in posterior cerebellum, p=0.0063 and p=0.0029, respectively) (Fig. 2M–P). Thus, IUGR moderately increases the number of undifferentiated GC precursors but leads to a dramatic accumulation of differentiating pre-migratory GCs in the EGL of SGA pigs at P0.

Intrauterine growth restriction increases proliferation and apoptosis in the EGL of newborn pigs.

During development, the size of progenitor pools depends on both the rates of proliferation and apoptosis. To assess proliferation in the EGL, we quantified phospho-Histone H3 (pH3)-immunoreactive (mitotic) cells (Sudarov and Joyner, 2007; Kim and Scot, 2014). Since our Pax6, Ki67, NeuN and Tag1 analyses (Fig. 2) revealed that IUGR similarly affects the EGL in the anterior and posterior cerebellum, data for anterior and posterior cerebellum were combined for pH3 and other subsequent analyses.

The number of pH3+ cells was increased in the EGL of P0 SGA pigs relative to NGA controls (p=0.034) (Fig. 3A–C). The proliferation of GC precursors in the EGL is positively regulated by Purkinje cells, which secrete Shh, the main mitogen for GCs (Dahmane and Ruiz i Altaba, 1999; Wallace, 1999; Wechsler-Reya and Scott, 1999; Fleming and Chiang, 2015). Consistent with an increased density of Purkinje cells (Fig. 1K–N), qRT-PCR analysis of laser capture microdissected EGL showed that expression of *Gli1* and *Ptch1* Shh-responsive genes (Iskusnykh et al., 2018) was significantly (p=0.016 for *Gli1* and p=0.034 for *Ptch1*) upregulated in the EGL of SGA cerebella (Fig. 3D–F).

Immunohistochemistry against activated Caspase 3 (act Casp3) was used to label apoptotic cells. There was a significant (p=0.0056) increase in the number of apoptotic cells in the EGL but not in the molecular layer or IGL of P0 SGA pigs (Fig. 3G–M), indicating that IUGR leads to elevated apoptosis specifically in the EGL.

To determine the identity of apoptotic cells in the EGL, we performed act Casp3/NeuN/DAPI co-labeling. This analysis revealed no difference in the number of apoptotic undifferentiated (NeuN-negative) GC precursors in the outer EGL but a dramatic (~2.5 fold, p=0.0012) increase in the number of apoptotic differentiating pre-migratory (NeuN+) GCs in the inner EGL of SGA pigs relative to NGA controls (Fig. 3N–Q). Taken together, our

data indicate that IUGR not only promotes proliferation of GC progenitors but also leads to an increased apoptosis of differentiating pre-migratory GCs in the EGL.

Intrauterine growth restriction disrupts the exit of granule cells from the EGL and reduces the expression of pro-migratory genes in the EGL of newborn pigs.

After exiting the cell cycle, GCs migrate radially from the EGL to their final destination in the IGL (Leto et al., 2016). The dramatic accumulation of differentiating GCs in the inner EGL (Fig. 2I–P) suggests a defect in the initiation of radial migration of these cells in SGA pigs. We analyzed GC migration by labeling proliferating GC precursors in the EGL with a BrdU pulse and following their location in organotypic cerebellar slices, which recapitulate many aspects of *in vivo* cerebellar development (Famulski et al., 2010; Iskusnykh et al., 2018). GC proliferation is limited to the EGL. Thus, using BrdU, which is incorporated into the DNA of cells in the S-phase of the cell cycle, is an appropriate approach to label GC progenitors for subsequent analysis of their distribution (Faust et al., 2003; Estep et al., 2018). 24 h after a BrdU pulse, a vast majority of BrdU-labeled cells remained in the EGL in cerebellar slices obtained from both NGA and SGA P0 pigs, and the average distance of BrdU+ cells from the outer cerebellar surface was not significantly different between NGA and SGA slices (Fig. 4A–C). 48 h after the beginning of a BrdU pulse, however, many BrdU + cells exited the EGL in slices from NGA pigs (Fig. 4D, arrows). In contrast, in cerebellar slices from SGA pigs, even 48 h after a BrdU pulse, virtually all BrdU+ cells were still found within the EGL or at the boundary between the EGL and the molecular layer (Fig. 4E, arrows). The average distance of BrdU+ cells from the outer cerebellar surface at 48 h was significantly ($p=2.9\times10^{-8}$) shorter in SGA slices relative to NGA slices (Fig. 4D–F), which is consistent with a disrupted migration from the EGL.

To identify potential migratory molecular mechanisms affected by IUGR, we analyzed the expression of pro-migratory genes *JamC*, *Pard3a*, *Sema6A*, *PlexinA2*, *Astn1*, *Barhl1*, and *Cxcr4* (Leto et al., 2016; Famulski et al., 2010; Singh and Solecki, 2015; Li et al., 2004; Huang et al., 2014) by qRT-PCR in the EGL isolated by laser capture microdissection from P0 NGA and SGA cerebella. There was a significant downregulation of *JamC* (encoding the junctional adhesion molecule C), *Pard3a* (encoding a Par-3 Family Cell Polarity Regulator), and *Sema6a* (encoding Semaphorin 6A) expression in the SGA relative to NGA EGL ($p=0.0038$ for *JamC*, $p=0.0009$ for *Pard3a*, $p=0.02$ for *Sema6a*). (Fig. 5A–C). In contrast, expression of *PlexinA2* (encoding a member of the plexin-A family of semaphorin co-receptors), *Astn1* (encoding Astrotactin 1), *Barhl1* (encoding BarH-like Homeobox 1), and *Cxcr4* (encoding C-X-C motif chemokine receptor 4) did not differ between SGA and NGA pigs (Fig. 5D–G). Thus, possible migration abnormalities in newborn SGA pigs were associated with a decreased expression of *JamC*, *Pard3a*, and *Sema6a* pro-migratory genes in GCs.

Accumulation of pre-migratory granule cells, disrupted expression of pro-migratory genes, and elevated apoptosis persisted over postnatal development in SGA pigs.

To determine whether GC abnormalities detected in SGA pigs at P0 persisted or resolved during postnatal development, we reared newborn SGA and NGA littermates for 20 days, feeding a milk replacer. Ki67 and pH3 immunohistochemistry revealed no difference in the

EGL between SGA and NGA pigs at P20 (Fig. 6A–G). In contrast, excessive accumulation of pre-migratory Tag1+ cells detected in SGA pigs at P0 persisted at P20 (p=0.0006 for anterior and p=0.019 for posterior cerebellum, respectively) (Fig. 6H–K), as well as a reduced expression of pro-migratory genes *JamC* and *Pard3a*, revealed by qRT-PCR analysis of laser capture microdissected EGL (p=0.024 for *JamC*, p=0.047 for *Pard3a*) (Fig. 6L–N). Similarly, increased apoptosis was also detected in the EGL of P20 SGA pigs relative to NGA littermates (p=0.039) (Fig. 6O–Q). Thus, while increased proliferation in the EGL spontaneously resolved during postnatal development, excessive accumulation of pre-migratory GCs, reduced expression of pro-migratory *JamC* and *Pard3a*, and increased apoptosis in the EGL persisted for a prolonged period of time after the birth of SGA pigs.

JamC and *Pard3a* rescue delayed granule cell migration and elevated apoptosis caused by intrauterine growth restriction.

Since an excessive accumulation of pre-migratory GCs was a long-lasting deficit observed in IUGR-affected pigs, we investigated the mechanisms underlying this phenotype. Among the three pro-migratory genes we found downregulated in the EGL of SGA pigs, two (*JamC* and *Pard3a*) operate in the same molecular pathway that controls exit of GCs from the EGL (Famulski et al., 2010; Singh and Solecki, 2015). Thus, even a modest simultaneous reduction of expression of these genes could potentially lead to dramatic GC migratory defects.

To determine whether *JamC*/*Pard3a* contribute to the IUGR-induced distribution abnormalities, we tested whether elevating the expression of these genes was sufficient to rescue exit of GCs from the EGL in SGA cerebella. For this purpose, superficially located GC precursors in P0 SGA cerebella were electroporated with an expression vector encoding nuclear mCherry (*pCIG2-H2B-mCherry*) alone or together with *JamC* and/or *Pard3a* expression plasmids, after that, cerebella were sliced and cultured *ex vivo*. NGA cerebella electroporated with *mCherry* served as controls. Confirming the results of our BrdU-labeling experiments (Fig. 4), when electroporated with *mCherry* alone, many targeted GCs in NGA slices had radially migrated from the EGL 48 h after electroporation (Fig. 7A, arrows). In contrast, under the same conditions, virtually all electroporated cells were found in the EGL in slices from SGA cerebella (Fig. 7B, arrowhead), and the average distance of mCherry+ GCs from the outer cerebellar surface was significantly shorter in slices from SGA relative to NGA pigs ($p=2.5\times10^{-7}$, Fig. 7F). Electroporation of SGA cerebella with *JamC* or *Pard3a* resulted in some electroporated (mCherry+) cells exiting the EGL (Fig. 7C, D, arrows), but the average distance of mCherry+ cells from the outer cerebellar surface was still not significantly different between *JamC* or *Pard3a*-electroporated SGA slices and SGA slices electroporated with *mCherry* alone (Fig. 7F). However, co-electroporation of SGA cerebella with *JamC+Pard3a*, dramatically increased the number of mCherry+ cells located beyond the EGL (Fig. 7B–E). Moreover, the average distance of mCherry+ cells from the outer cerebellar surface was significantly ($p=1.1\times10^{-11}$) increased in SGA slices co-electroporated with *JamC+Pard3a* relative to SGA slices electroporated with *mCherry* (Fig. 7F). Thus, elevated expression of *JamC* combined with *Pard3a*, but not of either gene alone, efficiently increased the number of GCs located beyond the EGL in SGA slices, 48 h after electroporation.

Notably, 48 h after electroporation, co-overexpression of *JamC* and *Pard3a* significantly (p=0.024) reduced the number of apoptotic cells in the EGL of SGA slices relative to those electroporated with *mCherry* alone (Fig. 7G–K), suggesting that normalizing expression of these genes was sufficient to rescue apoptosis of GCs, another key cerebellar phenotype observed in SGA pigs (Fig. 3G, H, K; 6O–K).

Our discovery of rescuing GCs from apoptosis by *JamC/Pard3a* prompted us to investigate how these genes rescue GC distribution defects in SGA slices in more detail. One possibility is that ectopic expression of *JamC+Pard3a* increases the number of GCs exited the EGL in SGA slices by simply promoting the survival of pre-migratory GCs. Alternatively, these genes directly regulate GC migration. To distinguish between these possibilities, we studied the dynamics of migration and apoptosis in our rescue experiments by analyzing electroporated slices at an earlier time point.

36 h after electroporation, mCherry+ GCs cells began exiting the EGL in control NGA slices and SGA slices co-electroporated with *JamC+Pard3a+mCherry*, but not in SGA slices electroporated with *mCherry* alone (Suppl. Fig. 1A–C). The average distance of mCherry+ cells from the outer cerebellar surface was already significantly increased in SGA slices co-electroporated with *JamC+Pard3a+mCherry* relative to SGA slices electroporated with *mCherry* alone (p=0.0001), and was not different relative to NGA slices electroporated with *mCherry* (Suppl. Fig. 1A–C, G). Interestingly, at this time, there was no difference in apoptosis yet between SGA slices co-electroporated with *JamC+Pard3a+mCherry* and those electroporated with *mCherry* alone (Suppl. Fig. 1D–F, H, I). Thus, in SGA slices 36 h after electroporation, *JamC+Pard3a* rescue only exit of GCs from the EGL but not apoptosis (Suppl. Fig. 1), revealing a direct role of *JamC/Pard3a* in the regulation of GC migration in our experimental system.

Discussion

IUGR increases the risk of development of motor and cognitive impairments (Colella et al., 2018; Vollmer and Edmonds, 2019). Patient imaging studies suggest that some of these deficits arise because of compromised cerebellar development, but the cellular and molecular mechanisms affected by IUGR remain poorly understood (Caetano et al., 2015; De Bie et al., 2011). Using the pig as a translational animal model, we found that the compromised initiation of radial migration of GCs, mediated by the JamC/ Pard3a molecular pathway, is a major contributor to the cerebellar pathology caused by IUGR.

Consistent with studies of SGA infants (Snijders et al., 1994; Caetano et al., 2015; De Bie et al., 2011), we showed that spontaneous IUGR in the pig reduces cerebellar weight, emphasizing the value of the pig as a translational animal model. At P0, SGA pigs revealed a reduced number of GCs in both anterior and posterior IGL. Since GCs comprise a large fraction of the cerebellar weight and volume (Chizhikov and Millen, 2020), a total reduction of cerebellar size in subjects born SGA results, at least partially, from the reduced number of GCs. Since GCs are critical for the proper functioning of cerebellum (Leto et al., 2016; Gill and Sillitoe, 2019), a reduction in the number of GCs likely contributes to the motor and cognitive deficits observed in SGA subjects as well.

Notably, the decreased number of mature GCs, which we describe in SGA pigs, has been reported in rat, guinea pig, and ovine studies, in which IUGR was achieved via ligation of uterine arteries in late pregnancy (Mallard et al., 2000; McDougal et al., 2017; Tolcos et al., 2018; Yawno et al., 2019). Thus, regardless of the species (pig, rat, guinea pig or sheep), timing (late versus early pregnancy) and the mode of induction of placental insufficiency (abrupt surgery versus natural chronic development), IUGR invariably reduces the number of mature GCs.

Cerebellar hypoplasia due to a decreased number of differentiated GCs is not unique to IUGR but has been described in other human conditions, including genetically caused cerebellar malformation disorders, such as Dandy-Walker malformation and Joubert syndrome, and also in subjects in which cerebellum was affected by non-genetic causes, such as preterm birth or drug exposure (Millen and Gleeson, 2008; Blank et al., 2011; Heine et al., 2011; Iskusnykh et al., 2018). In many of these conditions, a decreased number of GCs results from a reduced proliferation of GC precursors in the EGL because of compromised Shh signaling (in patients with Joubert syndrome, Dandy-Walker malformation, or those who received glucocorticoids) (Heine et al., 2011; Blank et al., 2011; Chizhikov et al., 2007; Spassky et al., 2008; Aguilar et al., 2012) or Jag1/Notch signaling (in subjects born preterm) (Iskusnykh et al., 2018). Surprisingly, despite a reduced number of GCs in the IGL of P0 SGA pigs, we observed increased rather than decreased proliferation in the EGL, which was associated with an upregulation of Shh-responsive genes *Gli1* and *Ptch1* and increased density of Purkinje cells, the main source of Shh in the cerebellum. Notably, proliferation of GC precursors is a complex process tightly regulated by multiple signaling pathways (Leto et al., 2016). Our data do not exclude a possibility that other mitogenic pathways, alone or in addition to the Shh pathway, contribute to the GC overproliferation in SGA pigs.

An increased number of PCs and/or elevated GC proliferation was not observed in previous uterine artery ligation studies, likely because for those studies, IUGR was induced late during pregnancy, after Purkinje cells have already been born. Alternatively, the sensitivity of the developing cerebellum to IUGR may be different between large animals and rodents, which were used in most previous IUGR studies (Mallard et al., 2000; McDougal et al., 2017; Tolcos et al., 2018). Regardless, the increase in proliferation in the EGL of SGA pigs was minor (the number of Ki67+ GC precursors was increased by only 12–18% in P0 SGA pigs) and transient, being spontaneously normalized during postnatal life.

In contrast to transient overproliferation of GCs, we detected two long-lasting phenotypes in SGA cerebella: a dramatic accumulation of pre-migratory GCs and an increased apoptosis, predominantly affecting these cells in the EGL. Accumulation of pre-migratory cells in the inner EGL of SGA pigs suggests a compromised exit of GCs from this germinal zone, which we confirmed in organotypic cerebellar slice culture experiments. Although direct analysis of GC migration was not performed in previously published IUGR studies, an increased EGL thickness with a greater density of Ki67-negative (post-mitotic) cells was reported in guinea pigs affected by IUGR resulting from uterine artery ligation, suggesting compromised exit of GCs from the EGL in that model system as well (Tolcos et al., 2018).

GCs radially migrate from the EGL to IGL along Bergmann glial fibers, and both intrinsic molecules and the availability of Bergmann glial fibers are critical for proper radial migration of GCs (Leto et al., 2016). In P0 SGA cerebella, we found a reduced number of Bergmann glial fibers. To determine whether IUGR also affects intrinsic molecules that regulate exit of GCs from the EGL, we assayed expression of key migratory genes in the EGL isolated by laser capture microdissection and found that three pro-migratory genes, *JamC*, *Pard3a*, and *Sema6a,* were downregulated in SGA pigs. Interestingly, two of these proteins, JamC and Pard3a, function in the same molecular pathway (Famulski et al., 2010; Leto et al., 2016), suggesting that the reduced activity of the JamC/Pard3a pathway in GCs contributes to GC distribution abnormalities in SGA cerebella. JamC is an adhesion molecule. To be functionally active, JamC needs to be positioned at the cell membrane, which is achieved via its interaction with a Pard3a-containing protein complex (Leto et al., 2016). Using electroporation of organotypic slices from SGA pigs, we showed that despite a reduced density of Bergmann glial fibers, increasing the combined expression of *JamC* and *Pard3a* in GCs was sufficient to rescue exit of GCs from the EGL, identifying downregulation of expression of these two genes as a major cause of GC migration abnormalities in IUGR-affected cerebella. Notably, individual electroporation of *Pard3a* and *JamC* resulted in a much more limited rescue of GC exit from the EGL as compared to co-electroporation of these genes, emphasizing that cooperation of these proteins is necessary to rescue IUGR-affected GC migration.

Interestingly, in SGA slices analyzed 48 h after electroporation, *JamC+Pard3a* rescued not only the exit of GCs from the EGL but also normalized apoptosis. Importantly, in these SGA slice experiments, *JamC*/*Pard3a* rescued the GC exit as early as 36 h after electroporation, while apoptosis has not become normalized until a later stage, revealing a direct involvement of the JamC/Pard3a pathway into the regulation of GC migration in our experimental system. Disruption of JamC/Pard3a-dependent GC migration is also consistent with the accumulation of pre-migratory GCs in the inner EGL of SGA cerebellum *in vivo*, the phenotype that could not be explained by an elevated apoptosis alone.

Because in our *JamC*/*Pard3a* SGA rescue experiments, improved migration preceded the normalized apoptosis, it is possible that in IUGR-affected cerebella, apoptosis is a secondary consequence resulting from the abnormal expansion of the population of pre-migratory GCs in the EGL. However, we cannot exclude a possibility that *JamC/Pard3a*, in addition to regulating migration of GCs, also regulate survival of pre-migratory GCs via migration-independent mechanisms. Regardless, since both excessive accumulation of pre-migratory GCs and elevated apoptosis are long-lasting phenotypes in the cerebellum of SGA pigs, it is likely that both disrupted radial migration and excessive death of GCs contribute to the reduced number of mature GCs (cerebellar hypoplasia) in the IGL of IUGR-affected cerebella.

It has been recently demonstrated that hypoxia reduces *JamC* expression in microvascular endothelial cells in both humans and mice (Burek et al., 2019). In addition, E3 ubiquitin-protein ligase Siah, which promotes proteasomal degradation of Pard3a protein, is activated by hypoxia in fibroblasts (Nakayama and Ronai, 2004). Thus, an IUGR-related decrease in the activity of the JamC/Pard3a pathway and the resulting disruption of GC migration and

increased apoptosis may be triggered by hypoxia, which is commonly associated with placental insufficiency in both humans and model organisms (Kovacs et al., 2019; Hutter et al., 2010).

In conclusion, using the pig as a translational animal model of a chronically developing early-onset IUGR (Ashworth et al., 2001; Radlowski et al., 2014), we recapitulated the reduced cerebellar growth observed in human patients and demonstrated that it was associated with a decrease in the number of mature GCs (cerebellar hypoplasia) in the IGL. Cerebellar hypoplasia is a common human phenotype that can arise from both genetic and non-genetic causes. While in many cases cerebellar hypoplasia is caused by a reduced proliferation of GC precursors (Millen and Gleeson, 2008; Blank et al., 2011; Heine et al., 2011; Iskusnykh et al., 2018), we report herein disrupted migration/elevated apoptosis of GCs as a distinct mechanism for cerebellar hypoplasia caused by early-onset IUGR. Previously, disruption of neuronal migration was observed in fetal alcohol syndrome (Komuro et al., 2014). In contrast to ethanol, which slows radial migration of GCs along the migratory pathway (Komuro et al., 2014), IUGR affects an earlier step – the exit of GCs from the EGL, acting via the neuronal cell adhesion JamC/Pard3a pathway. Recently, enhancing the proliferation of GC progenitors with a Shh agonist has been proposed as a treatment strategy for the cerebellar hypoplasia resulting from glucocorticoid exposure (Heine et al., 2011; Nguyen et al., 2018). Interestingly, we observed an overproliferation of GC precursors in the EGL of SGA pigs. This overproliferation, however, was obviously insufficient to prevent a reduction in the number of mature GCs, because supernumerous newborn GCs did not properly exit the EGL/become eliminated via apoptosis. Thus, we propose that activation of the JamC/Pard3 molecular pathway may be a promising strategy for the alleviation of cerebellar pathology in IUGR-affected patients, at least for those affected by an early-onset IUGR due to chronic placental insufficiency.

Supplementary Material

Refer to Web version on PubMed Central for supplementary material.

Acknowledgements:

We thank David Solecki (St. Jude Children's Research Hospital) for expression plasmids and advice regarding *ex-vivo* cerebellar electroporation, Donny Ray for procurement of experimental pigs, and Sergei Krat, Anastasia Zakharova, and Liliya Mukhametzyanova (University of Tennessee Health Science Center) for assistance with cerebellar slices. This work was supported by NIH R01 NS093009 and R21 NS077163 to V.V.C., and fellowships and a research grant from the Neuroscience Institute of the University of Tennessee Health Science Center to I.Y.I, N.F., and V.V.C.

Abbreviations:

IUGR	intrauterine growth restriction
SGA	small for gestational age
NGA	normal for gestational age
GCs	granule cells

EGL	external granule cell layer
IGL	internal granule cell layer
OCT	optimum cutting temperature compound
LCM	laser capture microdissection

References

1. Aguilar A, Meunier A, Strehl L, Martinovic J, Bonniere M, Attie-Bitach T, Encha-Razavi F, Spassky N (2012) Analysis of human samples reveals impaired SHH-dependent cerebellar development in Joubert syndrome/Meckel syndrome. Proc Natl Acad Sci USA 109: 16951–16956. [PubMed: 23027964]
2. Ashworth CJ, Finch A, Page K, Nwagwu M, McArdle H (2001) Causes and consequences of fetal growth retardation in pigs. Reprod Suppl 58: 233–246. [PubMed: 11980193]
3. Bamfo JE, Odibo A (2011) Diagnosis and management of fetal growth restriction. J Pregnancy 2011: 640715. [PubMed: 21547092]
4. Basson MA, Wingate RJ (2013) Congenital hypoplasia of the cerebellum: developmental causes and behavioral consequences. Front Neuroanat 7: 29. [PubMed: 24027500]
5. Blank M, Grinberg I, Aryee E, Laliberte C, Chizhikov V, Henkelman R, Millen K (2011) Multiple developmental programs are altered by loss of Zic1 and Zic4 to cause Dandy-Walker malformation cerebellar pathogenesis. Development 138: 1207–1216. [PubMed: 21307096]
6. Brown LD, Hay W (2016) Impact of placental insufficiency on fetal skeletal muscle growth. Mol Cell Endocrinol 435: 69–77. [PubMed: 26994511]
7. Buddington R, Chizhikov V, Iskusnykh I, Sable H, Sable J, Holloway Z, Blumenfeld Katzir T, Merwe M, Yakimkova T, Buddington K, Lifshitz Y, Tessler S, Gilbert A (2018) A Phosphatidylserine Source of Docosahexanoic Acid Improves Neurodevelopment and Survival of Preterm Pigs. Nutrients 10: 637.
8. Burek M, König A, Lang M, Fiedler J, Oerter S, Roewer N, Bohnert M, Thal S, Blecharz-Lang K, Woitzik J, Thum T, Förster C (2019) Hypoxia-Induced MicroRNA-212/132 Alter Blood-Brain Barrier Integrity Through Inhibition of Tight Junction-Associated Proteins in Human and Mouse Brain Microvascular Endothelial Cells. Transl Stroke Res 10: 672–683. [PubMed: 30617994]
9. Butts T, Green MJ, Wingate RJ (2014) Development of the cerebellum: simple steps to make a ‘little brain’. Development 141: 4031–41. [PubMed: 25336734]
10. Caetano AC, Zamarian A, Araujo Júnior E, Cavalcante R, Simioni C, Silva C, Rolo L, Moron A, Nardozza L (2015) Assessment of Intracranial Structure Volumes in Fetuses With Growth Restriction by 3-Dimensional Sonography Using the Extended Imaging Virtual Organ Computer-Aided Analysis Method. J Ultrasound Med 34: 1397–1405. [PubMed: 26206825]
11. Chizhikov VV, Davenport J, Zhang Q, Shih E, Cabello OA, Fuchs J, Yoder B, Millen K (2007) Cilia proteins control cerebellar morphogenesis by promoting expansion of the granule progenitor pool. J Neurosci 27: 9780–9789. [PubMed: 17804638]
12. Chizhikov VV, Iskusnykh I, Steshina E, Fattakhov N, Lindgren A, Shetty A, Roy A, Tole S, Millen K (2019) Early dorsomedial tissue interactions regulate gyrification of distal neocortex. Nat Commun 10: 5192. [PubMed: 31729356]
13. Chizhikov VV, Millen KJ (2020) Neurogenesis in the cerebellum In: Comprehensive Developmental Neuroscience (Rubenstein J, Rakic P, eds). Amsterdam: Elsevier (in press).
14. Colella M, Frérot A, Rideau Batista Novais A, Baud O (2018) Neonatal and Long-Term Consequences of Fetal Growth Restriction. Curr Pediatr Rev 14: 212–218. [PubMed: 29998808]
15. Currle DS, Cheng X, Hsu CM, Monuki ES (2005) Direct and indirect roles of CNS dorsal midline cells in choroid plexus epithelia formation. Development 132: 3549–3559. [PubMed: 15975937]
16. Dahmane N, Ruiz i Altaba A (1999) Sonic hedgehog regulates the growth and patterning of the cerebellum. Development 126: 3089–3100. [PubMed: 10375501]

17. Daza RA, Englund C, Hevner RF (2007) Organotypic slice culture of embryonic brain tissue. CSH Protoc. 2007: pdb.prot4914.
18. De Bie HM, Oostrom KJ, Boersma M, Veltman DJ, Barkhof F, Delemarre-van de Waal HA, van den Heuvel MP (2011) Global and Regional Differences in Brain Anatomy of Young Children Born Small for Gestational Age. PLoS One 6: e24116. [PubMed: 21931650]
19. Devaskar SU, Chu A (2016) Intrauterine Growth Restriction: Hungry for an Answer. Physiology 31: 131–146. [PubMed: 26889018]
20. Englund C, Kowalczyk T, Daza R, Dagan A, Lau C, Rose M, Hevner R (2006) Unipolar brush cells of the cerebellum are produced in the rhombic lip and migrate through developing white matter. J Neurosci 26: 9184–9195. [PubMed: 16957075]
21. Estep J, Wong W, Wong Y, Loui B, Riccomagno M (2018) The RacGAP β-Chimaerin is essential for cerebellar granule cell migration. Sci Rep 8: 680. [PubMed: 29330522]
22. Famulski J, Trivedi N, Howell D, Yang Y, Tong Y, Gilbertson R, Solecki DJ (2010) Siah regulation of Pard3A controls neuronal cell adhesion during germinal zone exit. Science 330: 1834–1838. [PubMed: 21109632]
23. Faust PL (2003) Abnormal cerebellar histogenesis in PEX2 Zellweger mice reflects multiple neuronal defects induced by peroxisome deficiency. J Comp Neurol 461: 394–413. [PubMed: 12746876]
24. Fauquier T, Chatonnet F, Picou F, Richard S, Fossat N, Aguilera N, Lamonerie T, Flamant F (2014) Purkinje cells and Bergmann glia are primary targets of the TRα1 thyroid hormone receptor during mouse cerebellum postnatal development. Development 141: 166–175. [PubMed: 24346699]
25. Fleming J, Chiang C (2015) The Purkinje neuron: A central orchestrator of cerebellar neurogenesis. Neurogenesis (Austin) 2: e1025940. [PubMed: 27604220]
26. Haldipur P, Dang D, Millen KJ (2018) Embryology. Handb Clin Neurol 154: 29–44. [PubMed: 29903446]
27. Haldipur P, Aldinger KA, Bernardo S, Deng M, Timms AE, Overman LM, Winter C, Lisgo SN, Razavi F, Silvestri E, Manganaro L, Adle-Biassette H, Guimiot F, Russo R, Kidron D, Hof PR, Gerrelli D, Lindsay SJ, Dobyns WB, Glass IA, Alexandre P, Millen KJ. (2019) Spatiotemporal expansion of primary progenitor zones in the developing human cerebellum. Science 366: 454–460. [PubMed: 31624095]
28. Heine VM, Griveau A, Chapin C, Ballard PL, Chen JK, Rowitch DH (2011) A small-molecule smoothened agonist prevents glucocorticoid-induced neonatal cerebellar injury. Sci Transl Med 3: 105ra104.
29. Herrera EA, Alegría R, Farias M, Díaz-López F, Hernández C, Uauy R, Regnault TR, Casanello P, Krause BJ (2016) Assessment of in vivo fetal growth and placental vascular function in a novel intrauterine growth restriction model of progressive uterine artery occlusion in guinea pigs. J Physiol 594: 1553–61. [PubMed: 26719023]
30. Huang G, Edwards A, Tsai C, Lee Y, Peng L, Era T, Hirabayashi Y, Tsai C, Nishikawa S, Iwakura Y, Chen SJ, Flint J (2014) Ectopic cerebellar cell migration causes maldevelopment of Purkinje cells and abnormal motor behaviour in Cxcr4 null mice. PLoS One. 9: e86471. [PubMed: 24516532]
31. Hutter D, Kingdom J, Jaeggi E (2010) Causes and Mechanisms of Intrauterine Hypoxia and Its Impact on the Fetal Cardiovascular System: A Review. Int J Pediatr 2010: 401323. [PubMed: 20981293]
32. Iskusnykh IY, Steshina EY, Chizhikov VV (2016) Loss of Ptf1a Leads to a Widespread Cell-Fate Misspecification in the Brainstem, Affecting the Development of sSomatosensory and Viscerosensory Nuclei. J Neurosci 36: 2691–2710. [PubMed: 26937009]
33. Iskusnykh IY, Buddington R, Chizhikov V (2018) Preterm birth disrupts cerebellar development by affecting granule cell proliferation program and Bergmann glia. Exp Neurol 306: 209–221. [PubMed: 29772246]
34. Gill JS, Sillitoe R (2019) Functional Outcomes of Cerebellar Malformations. Front Cell Neurosci 13: 441. [PubMed: 31636540]

35. Glaser J, Greene G, Hendricks S (2007) Stereology for biological research with a focus on neuroscience. Williston, USA: MBF press.
36. Kim BJ, Scott DA (2014) Mouse model reveals the role of RERE in cerebellar foliation and the migration and maturation of Purkinje cells. PLoS One 9: e87518. [PubMed: 24466353]
37. Komuro Y, Galas L, Lebon A, Raoult E, Fahrion JK, Tilot A, Kumada T, Ohno N, Vaudry D, Komuro H (2015) The role of calcium and cyclic nucleotide signaling in cerebellar granule cell migration under normal and pathological conditions. Dev Neurobiol 75: 369–387. [PubMed: 25066767]
38. Kovacs C, Deal Ceds. (2019) Maternal-Fetal and Neonatal Endocrinology: Physiology, Pathophysiology, and Clinical Management. San Diego, CA: Academic Press.
39. Koziol L, Budding D, Andreasen N, D'Arrigo S, Bulgheroni S, Imamizu H, Ito M, Manto M, Marvel C, Parker K, Pezzulo G, Ramnani N, Riva D, Schmahmann J, Vandervert L, Yamazaki T (2014) Consensus paper: the cerebellum's role in movement and cognition. Cerebellum 13: 151–177. [PubMed: 23996631]
40. Leto K et al. (2016) Consensus Paper: Cerebellar Development. Cerebellum 15: 789–828. [PubMed: 26439486]
41. Livak K, Schmittgen T (2001) Analysis of relative gene expression data using real-time quantitative PCR and the 2(-Delta Delta C(T)) Method. Methods 25: 402–408. [PubMed: 11846609]
42. Li S, Qiu F, Xu A, Price S, Xiang M (2004) Barhl1 regulates migration and survival of cerebellar granule cells by controlling expression of the neurotrophin-3 gene. J Neurosci 24: 3104–3114. [PubMed: 15044550]
43. Mallard C, Loeliger M, Copolov D, Rees S (2000) Reduced number of neurons in the hippocampus and the cerebellum in the postnatal guinea-pig following intrauterine growth-restriction. Neuroscience 100: 327–333. [PubMed: 11008170]
44. Matheson SM, Walling GA, Edwards SA (2018). Genetic selection against intrauterine growth retardation in piglets: a problem at the piglet level with a solution at the sow level. Genet Sel Evol. 50:46. [PubMed: 30227828]
45. McDougall AR, Wiradjaja V, Azhan A, Li A, Hale N, Wlodek M, Hooper S, Wallace M, Tolcos M (2017) Intrauterine Growth Restriction Alters the Postnatal Development of the Rat Cerebellum. Dev Neurosci 39: 215–227. [PubMed: 28448983]
46. Millen KJ, Gleeson JG (2008) Cerebellar development and disease. Curr Opin Neurobiol 18: 12–19. [PubMed: 18513948]
47. Miller S, Huppi P, Mallard C (2016) The consequences of fetal growth restriction on brain structure and neurodevelopmental outcome. J Physiol 594: 807–823. [PubMed: 26607046]
48. Nakayama K, Ronai Z (2004) Siah: new players in the cellular response to hypoxia. Cell Cycle 3: 1345–1347. [PubMed: 15492505]
49. Nguyen V, Sabeur K, Maltepe E, Ameri K, Bayraktar O, Rowitch DH (2018) Sonic Hedgehog Agonist Protects Against Complex Neonatal Cerebellar Injury. Cerebellum 17: 213–227. [PubMed: 29134361]
50. Radlowski EC, Conrad MS, Lezmi S, Dilger RN, Sutton B, Larsen R, Johnson R (2014) A neonatal piglet model for investigating brain and cognitive development in small for gestational age human infants. PLoS One 9: e91951. [PubMed: 24637829]
51. Renaud J, Chédotal A (2014) Time-lapse analysis of tangential migration in Sema6A and PlexinA2 knockouts. Mol Cell Neurosci 63: 49–59. [PubMed: 25284064]
52. Rozance PJ, Brown LD, Thorn SR, Anderson MS, Hay W (2016) Jr. Avery's Neonatology: Pathophysiology and Management of the Newborn 7th ed. Philadelphia, PA: Wolters Kluwer.
53. Sharma D, Shastri S, Sharma P (2016) Intrauterine Growth Restriction: Antenatal and Postnatal Aspects. Clin Med Insights Pediatr 10: 67–83. [PubMed: 27441006]
54. Sillitoe RV, Joyner AL (2007) Morphology, molecular codes, and circuitry produce the three-dimensional complexity of the cerebellum. Annu Rev Cell Dev Biol 23: 549–577. [PubMed: 17506688]
55. Singh S, Solecki DJ (2015) Polarity transitions during neurogenesis and germinal zone exit in the developing central nervous system. Front Cell Neurosci 9: 62. [PubMed: 25852469]

56. Snijders RJ, De Courcy-Wheeler RH, Nicolaides KH (1994) Intrauterine growth retardation and fetal transverse cerebellar diameter. Prenat Diagn 14: 1101–1105. [PubMed: 7899277]
57. Spassky N, Han Y, Aguilar A, Strehl L, Besse L, Laclef C, Ros M, Garcia-Verdugo J, Alvarez-Buylla A (2008) Primary cilia are required for cerebellar development and Shh-dependent expansion of progenitor pool. Dev Biol 317: 246–259. [PubMed: 18353302]
58. Sudarov A, Joyner AL (2007) Cerebellum morphogenesis: the foliation pattern is orchestrated by multi-cellular anchoring centers. Neural Dev 2: 26. [PubMed: 18053187]
59. Swanson DJ, Steshina E, Wakenight P, Aldinger K, Goldowitz D, Millen K, Chizhikov V (2010) Phenotypic and genetic analysis of the cerebellar mutant tmgc26, a new ENU-induced ROR-alpha allele. Eur J Neurosci 32: 707–716. [PubMed: 20722722]
60. Tolcos M, McDougall A, Shields A, Chung Y, O'Dowd R, Turnley A, Wallace M, Rees S (2018) Intrauterine Growth Restriction Affects Cerebellar Granule Cells in the Developing Guinea Pig Brain. Dev Neurosci 40: 162–174. [PubMed: 29763885]
61. Vollmer B, Edmonds C (2019) School Age Neurological and Cognitive Outcomes of Fetal Growth Retardation or Small for Gestational Age Birth Weight. Front Endocrinol 10: 186.
62. Wallace V (1999) Purkinje-cell-derived Sonic hedgehog regulates granule neuron precursor cell proliferation in the developing mouse cerebellum. Curr Biol 9: 445–448. [PubMed: 10226030]
63. Wang Y, Fu W, Liu J (2016) Neurodevelopment in children with intrauterine growth restriction: adverse effects and interventions. J Matern Fetal Neonatal Med 29: 660–668. [PubMed: 25758617]
64. Wang J, Feng C, Liu T, Shi M, Wu G, Bazer F (2017) Physiological alterations associated with intrauterine growth restriction in fetal pigs: Causes and insights for nutritional optimization. Mol Reprod Dev 84: 897–904. [PubMed: 28661576]
65. Wechsler-Reya RJ, Scott MP (1999) Control of neuronal precursor proliferation in the cerebellum by Sonic Hedgehog. Neuron 22: 103–114. [PubMed: 10027293]
66. Yawno T, Sutherland A, Pham Y, Castillo-Melendez M, Jenkin G, Miller S (2019) Fetal Growth Restriction Alters Cerebellar Development in Fetal and Neonatal Sheep. Front Physiol 10: 560. [PubMed: 31191328]
67. Yeung J, Ha T, Swanson D, Goldowitz D (2016) A Novel and Multivalent Role of Pax6 in Cerebellar Development. J Neurosci 36: 9057–9069. [PubMed: 27581449]
68. Yoo J, Mak G, Goldowitz D (2014) The effect of hemorrhage on the development of the postnatal mouse cerebellum. Exp Neurol 252: 85–94. [PubMed: 24252180]
69. Zhang P, Ha T, Larouche M, Swanson D, Goldowitz D (2015) Kruppel-Like Factor 4 Regulates Granule Cell Pax6 Expression and Cell Proliferation in Early Cerebellar Development. PLoS One 10: e0134390. [PubMed: 26226504]

Highlights:

- IUGR reduces the number of mature granule neurons in the cerebellum.
- IUGR increases apoptosis and delays migration of granule cells from the EGL.
- IUGR reduces expression of pro-migratory genes JamC, Pard3a, and Sema6A in the EGL.
- JamC/Pard3a rescue migration and apoptosis of granule cells in the IUGR-affected cerebellum.

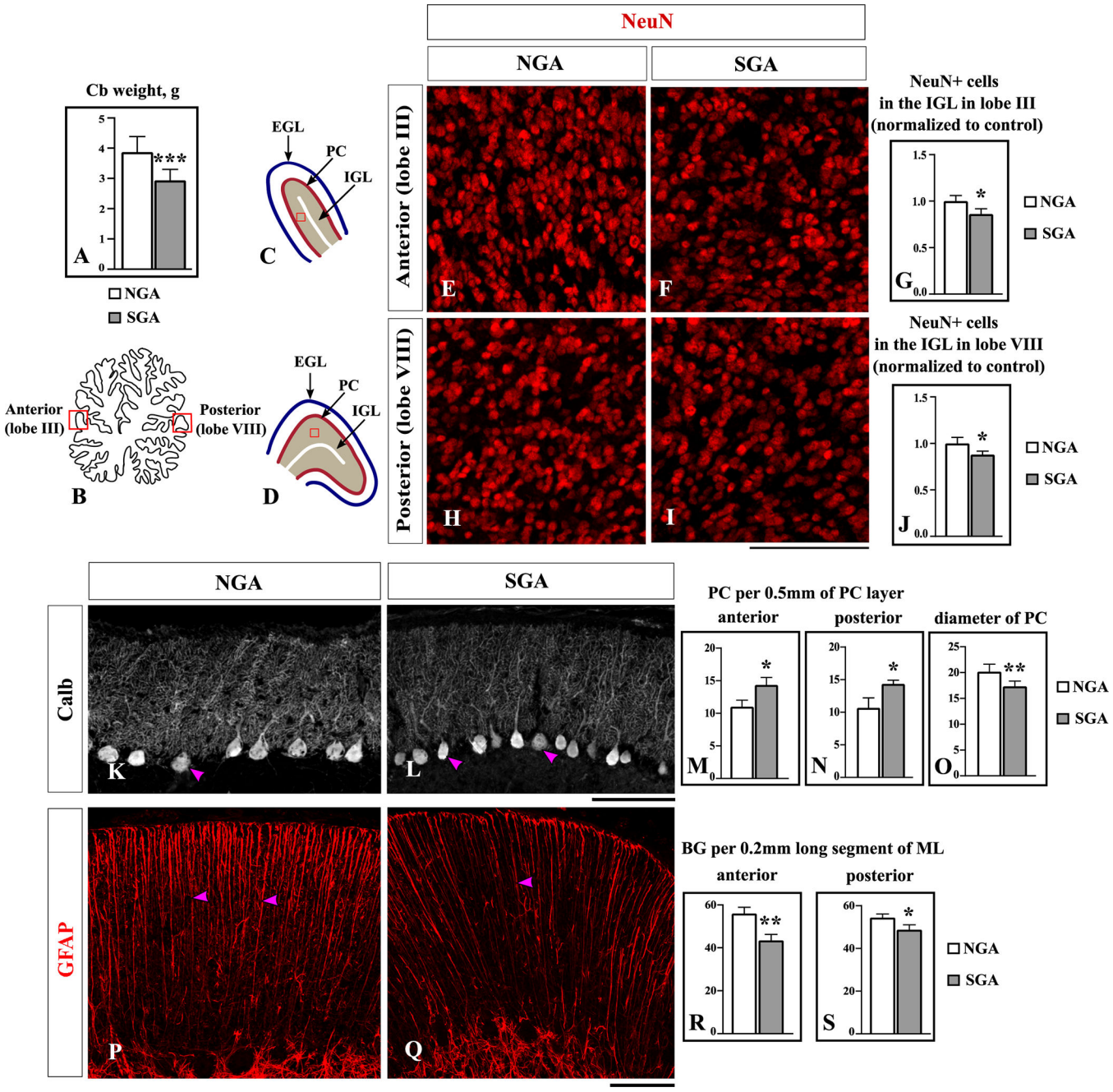

Fig. 1. Reduced numbers of granule cells and Bergmann glial fibers but increased density of Purkinje cells in the cerebellum of SGA pigs at P0.

(A) At P0, SGA pigs had a significantly reduced cerebellar weight relative to NGA pigs (t_{20}=4.97, p=7.4×10^{-5}, n=11 pigs per group). ***p<0.001.

(B-D) Schematic of a midsagittal section of pig cerebellar vermis (B). Diagrams C and D show higher magnification of anterior lobe III and posterior lobe VIII (the regions boxed in panel B), in which cells were quantified. (C, D) EGL - external granule cell layer, PC - Purkinje cell layer, IGL – internal granule cell layer.

(E-J) Panels E, F, H, and I show NeuN-immunostained IGL that corresponds to the regions boxed in adjacent diagrams C and D. (G, J) Quantification revealed a reduced number of NeuN+ GCs in the IGL in both anterior lobe III and posterior lobe VIII in SGA pigs relative to NGA controls (t_4=2.89, p=0.045 for lobe III and t_4=2.8, p=0.049 for lobe VIII, n=3 pigs per group). *p < 0.05.

(K, L) Calbindin immunostained Purkinje cells (arrowheads) in anterior (lobe III) cerebellum.

(M-O) Quantification of Purkinje cells. The higher density of Purkinje cells was detected in SGA relative to NGA pigs in both anterior (lobe III) (M) and posterior (lobe VIII) (N) cerebellum (t_4=3.78, p=0.019 for lobe III and t_4=3.89, p=0.018 for lobe VIII, n=3 pigs per group). The diameter of Purkinje cells was reduced in SGA relative to NGA cerebellum (O) (t_{10}=3.86, p=0.0032, n=6 pigs per group). **p < 0.01, *p < 0.05.

(P, Q) GFAP immunostained Bergmann glial fibers (arrowheads) in the anterior (lobe III) cerebellum. The density of GFAP+ Bergmann glial fibers was reduced in SGA relative to NGA pigs in both anterior (lobe III) (R) and posterior (lobe VIII) (S) cerebellum (t_4=5.32, p=0.006 for lobe III and t_4=3.44, p=0.026 for lobe VIII, n=3 pigs per group). **p < 0.01, *p < 0.05.

All data are means ± sd, all statistical values are from two-tailed t-test. Scale bars: 100 μm (E, F, H, I, K, L), 50 μm (P, Q).

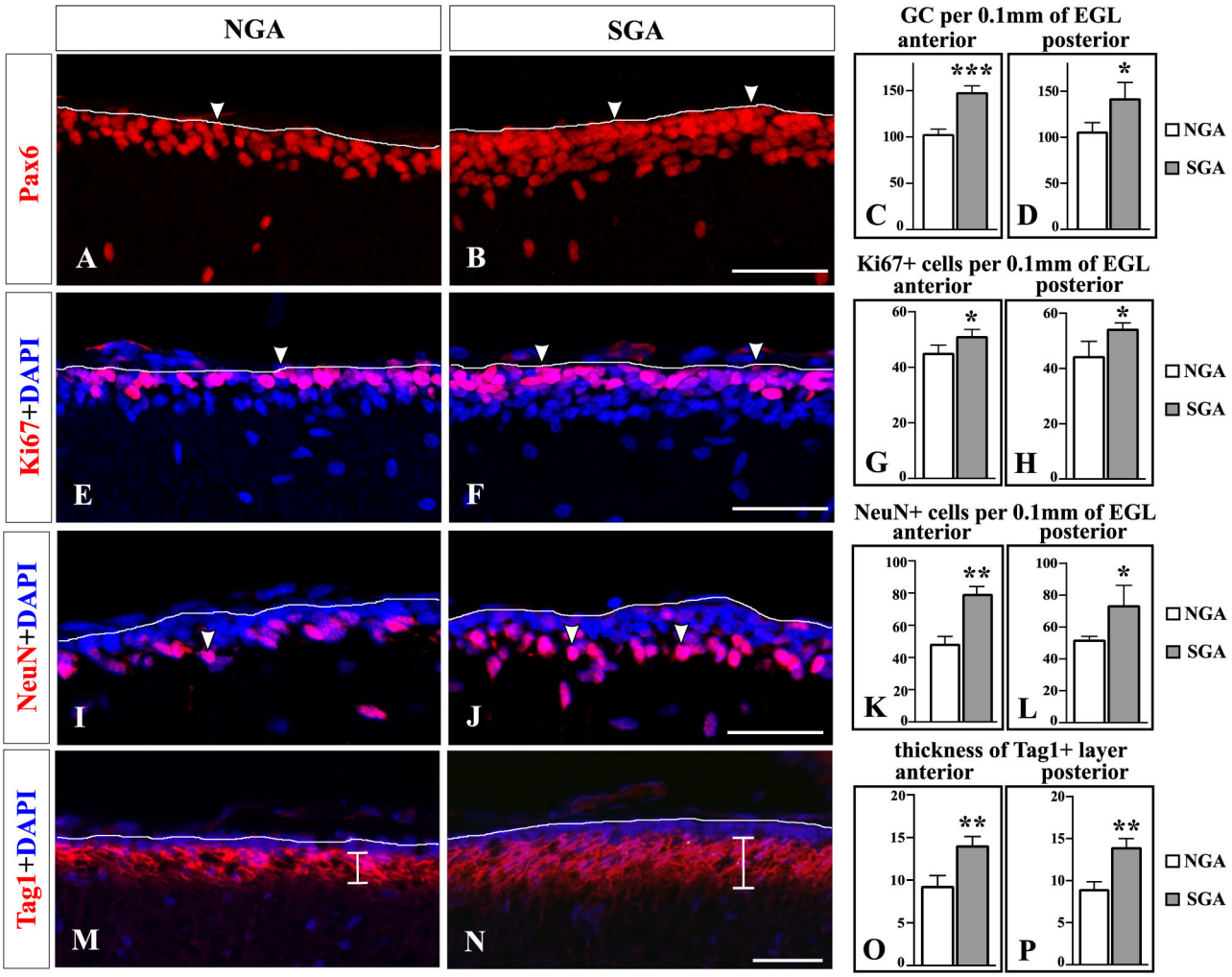

Fig. 2. Increased number of undifferentiated and differentiating granule cell precursors in the EGL of SGA pigs at P0.

(A, B, E, F, I, J, M, N) Sagittal sections of medial vermis, showing EGL in lobe III, stained with indicated antibodies. (C, D, G, H, K, L, O, P) Cells or thickness of the internal EGL were quantified in anterior (lobe III) and posterior (lobe VIII) cerebellum in P0 NGA and SGA pigs.

(A-D) Arrowheads point to Pax6+ GC precursors in the EGL (A, B) that were increased in the number in SGA relative to NGA pigs in both anterior and posterior cerebellum (C, D) (t_4=9.09, p=0.0008 for lobe III and t_4=3.17, p=0.034 for lobe VIII, n=3 pigs per group). ***p < 0.001, *p <0.05.

(E-H) Arrowheads point to undifferentiated Ki67+ GC precursors in the EGL (E, F) that were increased in the number in SGA relative to NGA pigs in both anterior and posterior cerebellum

(G, H) (t_4=2.9, p=0.044 for lobe III and t_4=3.05, p=0.038 for lobe VIII, n=3 pigs per group). *p <0.05.

(I-L) Arrowheads point to differentiating NeuN+ GC precursors in the EGL (I, J) that were increased in the number in SGA relative to NGA pigs in both anterior and posterior cerebellum

(K, L) (t_4=8.37, p=0.0011 for lobe III and t_4=3.01, p=0.04 for lobe VIII, n=3 pigs per group). **p < 0.01, *p <0.05.
(M-P) The thickness of the Tag1+ inner EGL (vertical bars in panels M, N) was increased in SGA relative to NGA pigs in both anterior and posterior cerebellum (O, P) (t_4=5.25, p=0.0063 for lobe III and t_4=6.5, p=0.0029 for lobe VIII, n=3 pigs per group). **p<0.01. All data are means ± sd, all statistical values are from two-tailed t-test.
Scale bars: 100 μm (A, B, E, F, I, J), 20 μm (M, N).

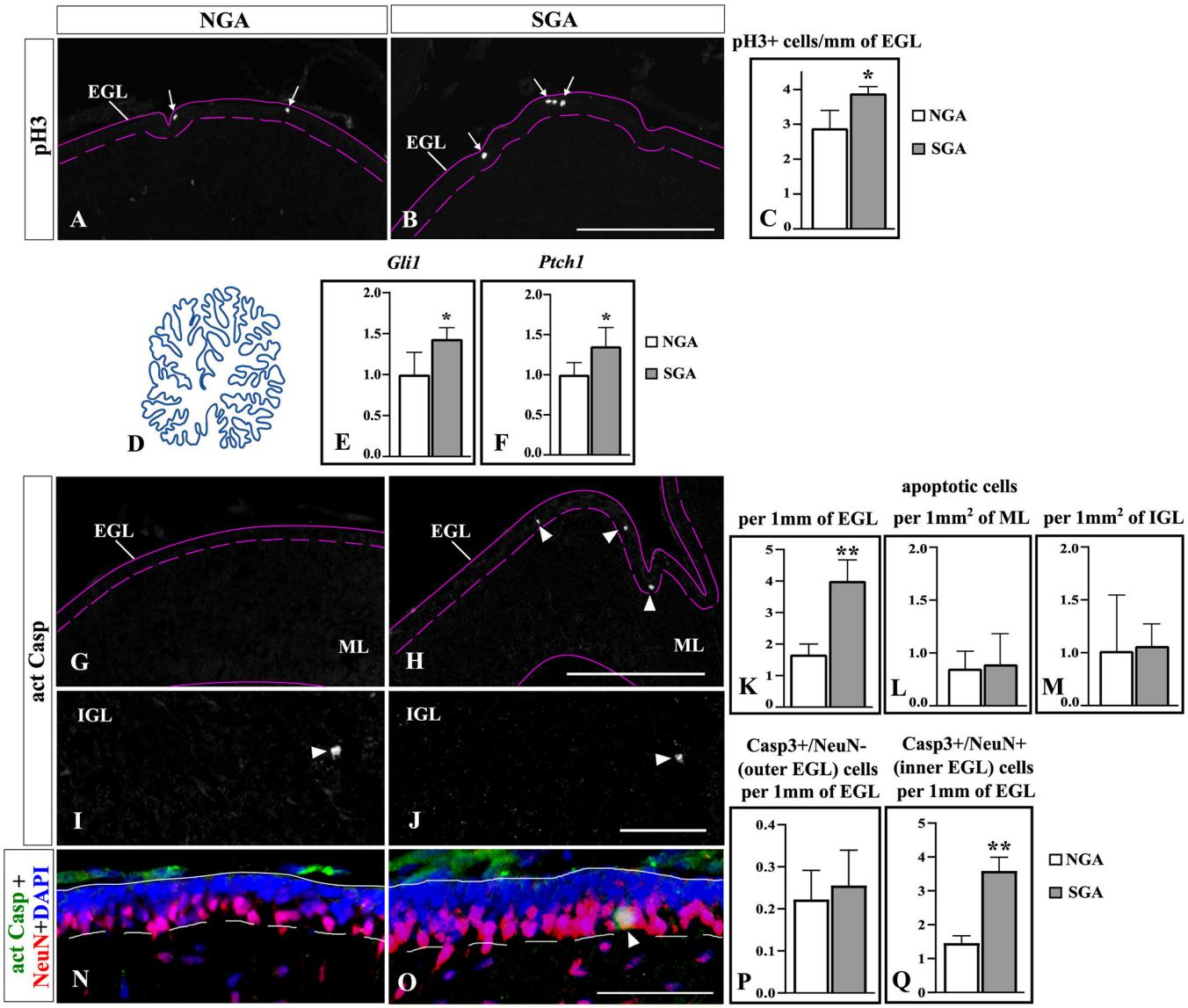

Fig. 3. Increased proliferation, apoptosis, and expression of Shh-regulated genes in the EGL of SGA pig cerebellum at P0.

(A, B, G-J, N, O) Sagittal sections of medial vermis stained with indicated antibodies. Panels A, B, N, O show the EGL, panels G, H show both the EGL and the molecular layer (ML), panels I, J show high magnification of the IGL. The outer and inner boundaries of the EGL are outlined by solid and dashed line, respectively (A, B, G, H, N, O). The lower solid line shows the lower boundary of the ML (G, H).

(A-C) Arrows point to mitotic (pH3+) cells in the EGL (A, B), that were increased in the number in SGA relative to NGA pigs (C) (t_4=3.18, p=0.034, n=3 pigs per group). *p <0.05.

(D-F) qRT-PCR analysis of *Gli1* and *Ptch1* expression in laser capture microdissected EGL (blue layer in the diagram D). *Gli1* and *Ptch1* expression (E, F) was significantly upregulated in the EGL of SGA pigs (t_7=3.15, p=0.016 for *Gli1* and t_7=2.63, p=0.034 for *Ptch1*, n=4 NGA and 5 SGA pigs). *p < 0.05.

(G-J) Arrowheads point to apoptotic (act Casp3+) cells in the EGL (G, H) or IGL (I, J). In SGA pigs, the number of apoptotic cells was increased in the EGL (t_4=5.42, p=0.0056) but not in the molecular layer or IGL (K-M). **p <0.01. n=3 pigs per group.
(N-Q) Arrowhead points to an apoptotic Casp3+/NeuN+ differentiating pre-migratory GC in the inner EGL in SGA cerebellum (O). Apoptotic cells were very rare in the outer (DAPI+/NeuN-negative) EGL in both NGA and SGA pigs, and no difference was detected between the two groups (N-P). In contrast, there was a dramatic increase in the number of apoptotic act Casp3+/NeuN+ differentiating pre-migratory cells in SGA cerebella (t_4=8.16, p=0.0012) (N, O, Q). **p <0.01. n=3 pigs per group.
All data are means ± sd, all statistical values are from two-tailed t-test.
Scale bar: 300 μm (panels A, B, G, H), 100 μm (panels I, J) and 80 μm (panels N, O).

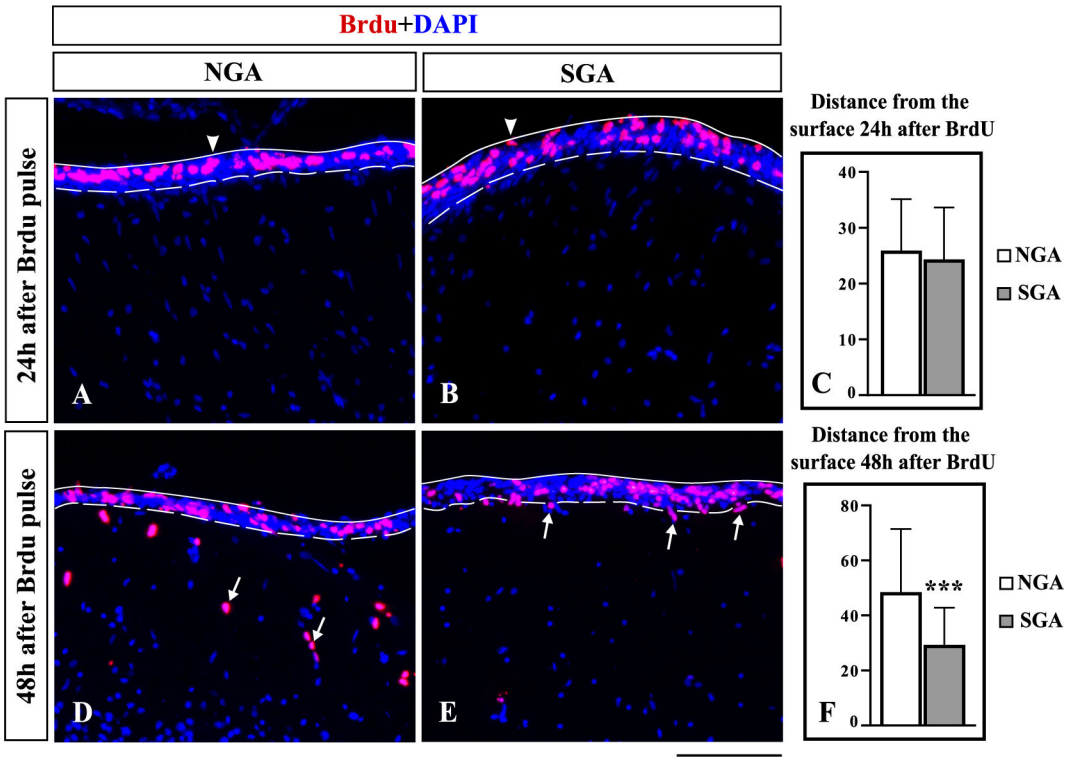

Fig. 4. Delayed exit of BrdU-labeled GCs from the EGL in organotypic cerebellar slices from P0 SGA pigs.

P0 pig cerebellar slices were pulsed with BrdU, cultured *in vitro*, and co-labeled with DAPI and anti-BrdU immunohistochemistry. The solid line shows the outer surface of the EGL, dashed line labels the inner boundary of the EGL.

(A-C) 24 h after a BrdU pulse, labeled GCs (arrowheads) were still located in the EGL, and there was no difference in the distance from the outer cerebellar surface between BrdU+ cells in slices from NGA and SGA pigs (C), n=4 slices per group, each slice was from an individual cerebellum.

(D-F) 48 h after a BrdU pulse, many BrdU+ cells in slices from NGA cerebella were located beyond the EGL, deep in the molecular layer (D, arrows). In contrast, virtually all BrdU+ cells in slices from SGA cerebella were found in the EGL, with few BrdU+ cells located at the boundary between the EGL and the molecular layer (E, arrows). (F) The average distance of BrdU+ cells from the outer cerebellar surface was significantly shorter in SGA slices compared to NGA slices 48 h after a BrdU pulse (t_{132}=5.9, p=2.9×10^{-8}, n=134 BrdU+ cells from 4 slices per group, each slice was from an individual cerebellum), suggesting a delayed migration of GCs from the EGL. ***p < 0.001. Data are means ± sd, all statistical values are from two-tailed t-test.

Scale bar: 100 μm.

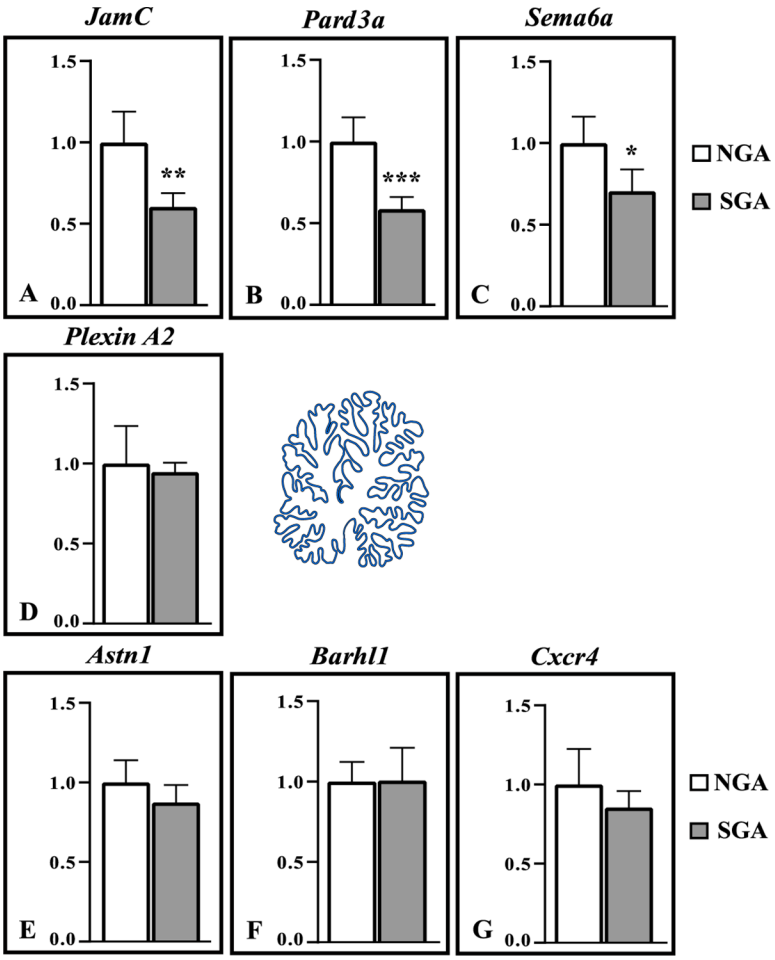

Fig. 5. Reduced expression of promigratory genes *JamC*, *Pard3a*, and *Sema6a* in the EGL of SGA pigs at P0.

qRT-PCR analysis of *JamC* (A), *Pard3a* (B), *Sema6a* (C), *Plexin A2* (D), *Astn1* (E), *Barhl1* (F), and *Cxcr4* (G) gene expression in laser capture microdissected EGL (blue layer in the diagram). *JamC*, *Pard3a*, and *Sema6a* were significantly downregulated in the EGL of P0 SGA pigs (t_7=4.24, p=0.0038 for *JamC*, t_7=5.51, p=0.0009 for *Pard3a*, and t_7=3, p=0.02 for *Sema6a*). ***p < 0.001, **p < 0.01, *p <0.05. Expression of *Plexin A2*, *Astn1*, *Barhl1*, and *Cxcr4* was not different between NGA and SGA EGL at P0. n = 4 NGA cerebella and n = 5 SGA cerebella. All data are means ± sd, all statistical values are from two-tailed t-test.

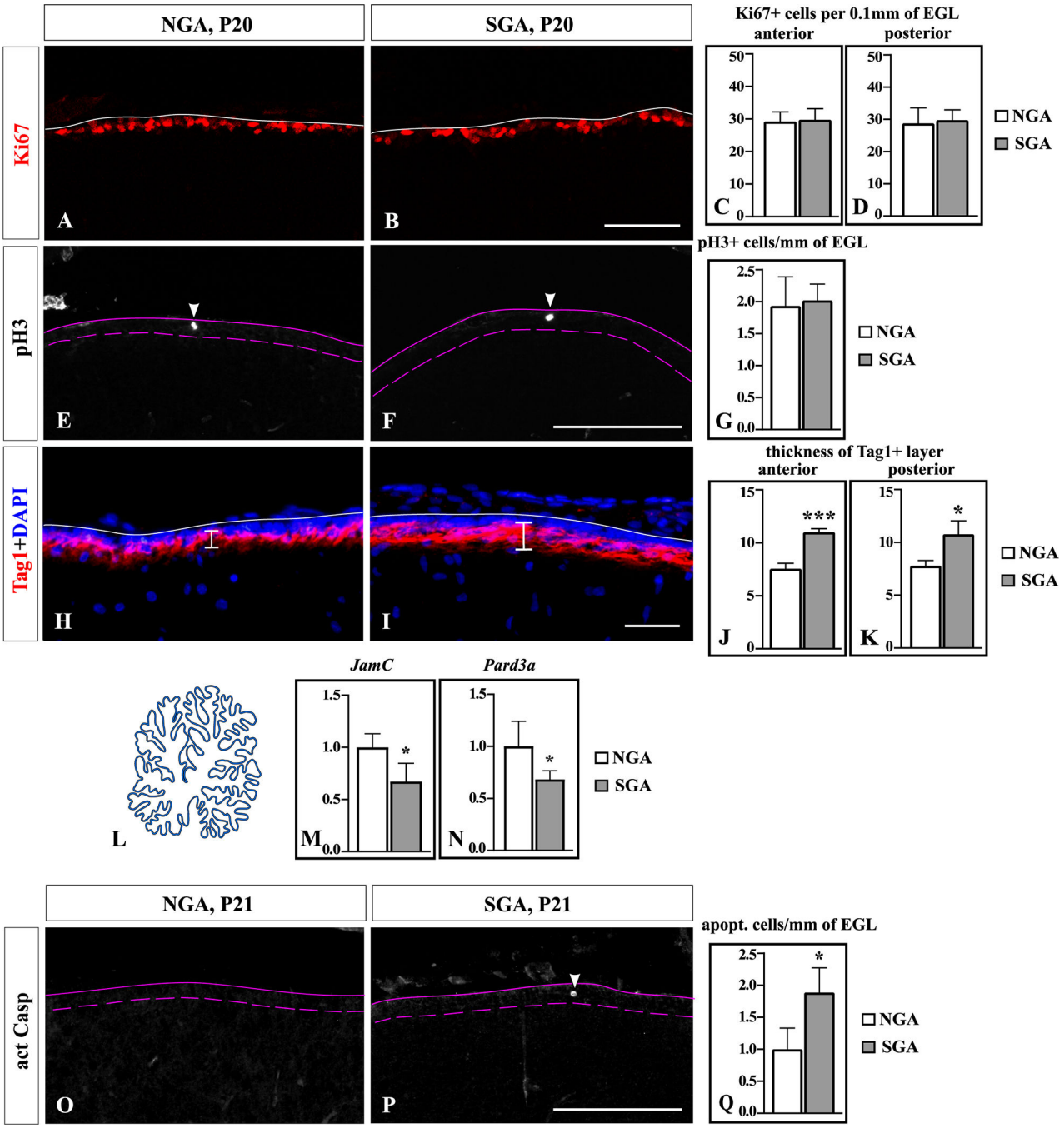

Fig. 6. Cellular and gene expression abnormalities in the EGL of SGA pigs at P20.

(A, B, E, F, H, I, O, P) Sagittal sections of P20 medial vermis that show EGL of lobe III, stained with indicated antibodies (alone or together with DAPI). Solid lines show the outer surface of the cerebellum. Dashed lines show the inner boundary of the EGL. (C, D, G, J, K, Q) Cells or thickness of the internal EGL were quantified separately in anterior (lobe III) and posterior (lobe VIII) cerebellum (in the regions depicted by red boxes in Fig. 1B) (C, D, J, K) or combined in anterior and posterior cerebellum (G, Q) in NGA and SGA pigs.

(A-D) There was no difference in the number of Ki67 + (undifferentiated) GC precursors in SGA relative to NGA pigs in both anterior and posterior cerebellum at P20. n=3 pigs per group.
(E-G) Arrowheads point to mitotic (pH3+) cells in the EGL (E, F), the number of which did not differ between SGA and AGA pigs at P20 (G). n=3 pigs per group.
(H-K) Thickness of the Tag1+ inner EGL (vertical bars in panels H, I) was increased in SGA relative to NGA pigs in both anterior and posterior cerebellum at P20 (J, K) (t_4=9.8, p=0.0006 for lobe III and t_4=3.82, p=0.019 for lobe VIII, n=3 pigs per group). ***p < 0.001, *p <0.05.
(L-N) qRT-PCR analysis of *JamC* (M) and *Pard3a* (N) expression in laser capture microdissected EGL (blue layer in the diagram L). Both genes were significantly downregulated in the EGL of SGA pigs at P20 (t_6=3, p=0.024 for *JamC*, t_6=2.49, p=0.047 for *Pard3a,* n=4 pigs per group). *p <0.05.
(O-Q) Arrowheads point to apoptotic (act Casp3+) cells (O, P) in the EGL that were increased in the number in SGA relative to NGA pigs at P20 (Q) (t_4=3.02, p=0.039, n=3 pigs per group). *p <0.05.
All data are means ± sd, all statistical values are from two-tailed t-test.
Scale bars: 100 μm (A, B), 300 μm (E, F, O, P), 20 μm (H, I).

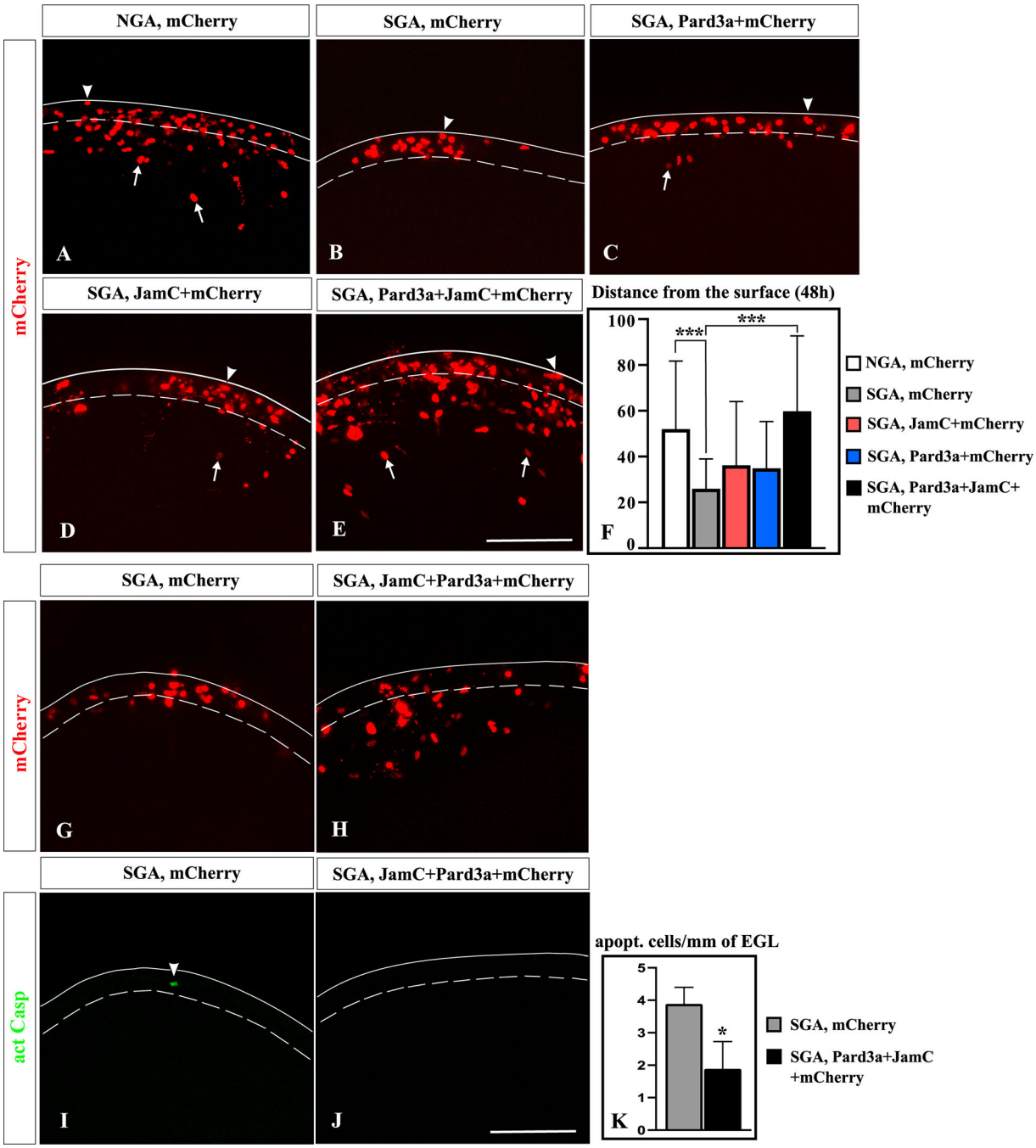

Fig. 7. 48 hours after electroporation, *JamC* and *Pard3a* rescue granule cell migration and apoptosis in the EGL of organotypic cerebellar slices from SGA pigs.

(A-E, G-J) P0 NGA or SGA cerebellar slices electroporated into the EGL with *mCherry* alone or together with indicated genes and cultured for 48 h. The solid line marks the outer surface of the EGL, the dashed line shows the inner boundary of the EGL. The red signal corresponds to the mCherry fluorescence in electroporated cells.

(A) In slices prepared from P0 NGA cerebella electroporated with *mCherry*, some electroporated cells remained in the EGL (arrowhead), while others radially migrated from the EGL (arrows).

(B) In slices prepared from P0 SGA cerebella electroporated with *mCherry*, virtually all electroporated cells remained in the EGL (arrowhead). (C-E) In SGA slices electroporated with *JamC, Pard3a*, or *Pard3a+JamC*, some electroporated cells remained in the EGL (arrowheads), while others (especially in slices co-electroporated with *Pard3a* and *JamC*) migrated out of the EGL (arrows). (F) The average distance of mCherry+ cells from the outer cerebellar surface was significantly smaller in *mCherry*-electroporated SGA slices compared to NGA slices (one-way ANOVA followed by Tukey's post hoc test, $p=2.5\times10^{-7}$). Co-electroporation of SGA slices with *Pard3a* and *JamC*, but not electroporation with any of these genes alone, significantly increased the average distance of mCherry+ cells from the outer cerebellar surface (one-way ANOVA followed by Tukey's post hoc test, $p=1.1\times10^{-11}$), n=4 slices per condition. Each slice was from a different cerebellum. ***$p < 0.001$. (G-K) Panels G, I, and H, J show the same slices imaged for mCherry (G, H) and act. Casp3 immunohistochemistry (I, J). Co-electroporation of *JamC* and *Pard3a* reduced the number of apoptotic cells in the EGL of SGA pigs (two-tailed t-test, $t_4=3.53$, $p=0.024$), n=3 slices per condition. Each slice was from a different cerebellum. *$p < 0.05$. Data are means ± sd. Scale bar: 100 μm.